Environ. Sci. Technol. **2003**, *37,* 5617−5624

Pore-Scale Analysis of Anaerobic Halorespiring Bacterial Growth along the Transverse Mixing Zone of an Etched Silicon Pore Network

INDUMATHI M. NAMBI, CHARLES J. WERTH,* ROBERT A. SANFORD, AND ALBERT J. VALOCCHI

Department of Civil and Environmental Engineering, University of Illinois at Urbana−Champaign, 205 North Mathews Avenue, Urbana, Illinois 61801

The anaerobic halorespiring microorganism, *Sulfurospirillum multivorans*, was observed in the pore structure of an etched silicon wafer to determine how flow hydrodynamics and mass transfer limitations along a transverse mixing zone affect biomass growth. Tetrachloroethene (PCE, an electron acceptor, 0.2 mM) and lactate (an electron donor, 2 mM) were introduced as two separate and parallel streams that mixed along a reaction line in the pore structure. The first visible biomass occupied a single line of pores in the direction of flow, a few pore bodies from the micromodel centerline. This growth was initially present as small aggregates; over time, these grew and fused to form finger-like structures with one end attached to downgradient ends of the silicon posts and the other end extending into pore bodies in the direction of flow. Biomass did not grow in pore throats as expected, presumably because shear forces were not favorable. Over the next few weeks, the line of growth migrated upward into the PCE zone and extended over a width of up to five pore spaces. When the PCE concentration was increased to 0.5 mM, the microbial biomass increased and growth migrated down toward the lactate side of the micromodel. A new analytical model was developed and used to demonstrate that transverse hydrodynamic dispersion likely caused the biomass to move in the direction observed when the PCE concentration was changed. The model was unable, however, to explain why growth migrated upward when the PCE concentration was initially constant. We postulate that this occurred because PCE, not lactate, sorbed to biofilm components and that biomass on the lactate side of the micromodel was limited in PCE. A fluorescent tracer experiment showed that biomass growth changed the water flow paths, creating a higher velocity zone in the PCE half of the micromodel. These results contribute to our understanding of biofilm growth and will help in the development of new models to describe this complex process.

Introduction

Groundwater contamination by organic solvents is a matter of serious concern in industrialized countries. In recent years, in situ anaerobic bioremediation has emerged as a promising approach to treat these compounds. Typically, an electron donor is mixed with water and injected into groundwater (*1*). This donor is carried in groundwater through and around the contaminant source (i.e., the electron acceptor), and where both the donor and acceptor mix, reductive dechlorination occurs. Alternative strategies involve placing or injecting immobile sources of electron donor upgradient of, within, or downgradient of a contaminant source zone (*2*, *3*). For example, a relatively immobile lactate polymer has been injected into groundwater to release hydrogen for reductive dechlorination (*4*). Immobile electron donor sources undergo hydrolysis and/or fermentation and release fatty acids and hydrogen to groundwater. As a result, these donors are carried in groundwater through and around the contaminant source and/or plumes.

Modeling studies indicate that injected nutrients are often consumed to depletion in the contaminant source zone or in the core of the plume where contaminant concentrations are highest (*5*, *6*). High contaminant concentrations may also be toxic to microorganisms. As a result, much of degradation occurs along the plume margins where contaminants mix with nutrients due to transverse dispersion (*6*). Modeling results indicate that the extent of transverse dispersion can control the longitudinal extent of a plume (*5*).

Transverse dispersion and its effects have been carefully studied in the absence of microbial growth (*7*−*10*). However, transverse dispersion and its effects have only recently been studied in the presence of microbial growth. Thullner et al. (*11*) observed biomass growth along transverse mixing zones between nitrate and glucose in a 2D glass flow-cell filled with a layer of glass beads. Biomass growth occurred as lines along the mixing zones. The biomass changed water flow patterns in the cell, showing that biomass growth in individual pores reduced the overall permeability. It follows that the morphology of biomass at the pore scale must affect permeability and subsequently transverse dispersion and contaminant degradation. Numerous studies performed with columns have shown that greater biomass correlates to lower permeability (*12*, *13*). Relatively few studies, however, have investigated the effects of biomass morphology on permeability, or the subsequent effects on transverse dispersion and contaminant degradation.

A variety of biomass morphologies have been observed in porous media, all under aerobic conditions; in some cases, these have been correlated to permeability and/or contaminant degradation rates. In several cases, thin layers or films of biomass were observed to cover real or model soil grains. These films were continuous or discontinuous depending on, among other factors, substrate loading (*14*). For example, under nutrient-rich conditions, biofilms were observed to thicken; in some pores biomass aggregates also formed. These thick films and aggregates blocked pore bodies and significantly decreased the permeability (*15*). Under nutrient-poor conditions, biomass sloughing occurred, resulting in a rebound of the permeability.

Biowebs and thin filaments have also been observed in porous media. Biowebs appeared like a spider web where each strand varied in size and shape (*16*). Biowebs blocked pores, caused flow diversion, and resulted in a decrease in permeability. Thin filaments were observed with aggregates in the same experiment (*17*). Filaments dominated growth at low pH, whereas biofilms and aggregates dominated at neutral pH. In a separate study, aggregate size was found to increase more in high flow zones where nutrient fluxes were

* Corresponding author phone: (217)333-3822; e-mail: werth@uiuc.edu.

10.1021/es034271w CCC: $25.00
Published on Web 11/11/2003

greater (*16*). Modeling results (*18*) suggest that aggregates cause a much greater decrease in the permeability than biofilms or filaments.

In only one study (*19*) was biomass growth at the pore scale correlated to biodegradation rates. Here, the biodegradation efficiency (one minus the ratio of effluent to influent concentration) decreased with increased substrate loading rates and increased flow velocities. Also, biofilm thickness decreased with increased distance from the inlet due to a reduction in nutrient levels. At low nutrient concentrations and flow velocities, biofilm thickness decreased while biodegradation efficiency increased. It was postulated that fewer pores were blocked at low nutrient conditions and that the biodegradation efficiency increased because degradation occurred in a greater number of pores.

While these studies have markedly improved our understanding of pore-scale biomass growth in porous media, significant questions remain. For example, what is the biomass morphology of anaerobic microorganisms in porous media, how does flow hydrodynamics affect biomass growth, and does biomass growth respond to nutrient mass transfer limitations along a transverse mixing zone? The goal of this paper is to determine the effects of flow hydrodynamics and mass transfer limitations along a transverse mixing zone on the growth of an anaerobic dechlorinating microorganism. Specifically, we want to test the hypotheses that anaerobic bacteria will grow in pore bodies and throats when nutrient conditions are favorable, that transverse hydrodynamic dispersion will control nutrient mixing and the location of microbial growth, and that biomass will reduce the permeability and therefore the extent of mixing between nutrients.

To test these hypotheses, the growth of an anaerobic halorespiring microorganism, *Sulfurospirillum multivorans* (formerly known as *Dehalospirillum multivorans*), was directly observed in the presence of different electron acceptor concentrations in a flow-through pore system etched into a silicon wafer. The electron acceptor (tetrachloroethene, PCE) and an electron donor (lactate) were introduced as two separate, parallel streams that mixed through transverse dispersion along a reaction line in the pore structure. As a result, growth was confined to a narrow transverse region of pores, and this allowed the response of biomass growth to the combined influences of flow hydrodynamics and nutrient mass transfer limitations to be assessed in a controlled way.

Experimental Methods

Bacteria and Growth Medium. *S. multivorans* was the only microorganism used in the experiments and was obtained from Dr. Frank Löffler of the Georgia Institute of Technology, Atlanta, GA. It is a Gram-negative, strictly anaerobic bacterium that is able to respire PCE via trichloroethene (TCE) to *cis*-1,2-dichloroethene (DCE) as a part of its energy metabolism (*20*). The culture was grown in 100 mL of anaerobic chloride-free basal medium in 160-mL serum bottles. The mineral salts medium was prepared and handled as previously described (*21*). The medium was adjusted to pH 7, transferred to serum bottles, and autoclaved prior to use. The medium was amended with 1 mL of Wolfe's vitamin solution. The medium was also amended with lactate as the carbon source and PCE as the electron acceptor to bring the solution concentrations to 2 and 0.2 mM, respectively. The Wolfe's vitamin solution, trace salts, and trace metal solutions were prepared as described by Sanford et al. (*21*).

Chemicals. PCE (99.9+%, Aldrich), TCE (99.5+%, Aldrich), and *cis*-1,2-DCE (97%, Aldrich) were used in all experiments and/or calibrations.

Micromodel Fabrication. The experiments were conducted in the silicon-based micromodel illustrated in Figure 1. The first micromodels used to study pore-scale microbial processes were constructed by etching glass (*22*); better

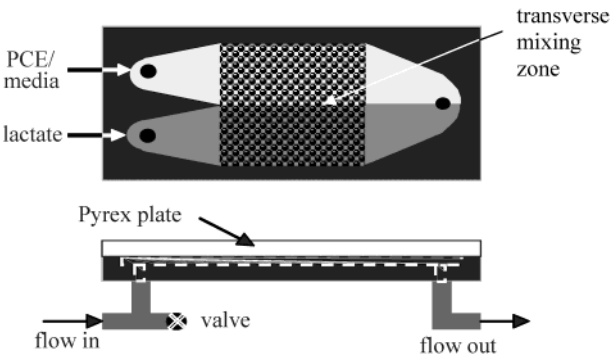

FIGURE 1. Illustration of micromodel system.

control of the pore network geometry is obtained by etching silicon. The micromodel is ~15 μm deep, and it contains a 1 cm × 1 cm close-packed array of ~300 μm diameter silicon posts separated by ~35 μm pore throats. The silicon posts are a two-dimensional representation of sand grains, and the etched regions between them the pore space. The close-packed configuration contains flow stagnation zones at the upstream and downstream end of each silicon post. Flow is highest in the pore throats and lowest in the pore bodies.

The close-packed pattern was etched into a silicon wafer using a standard wet etching technique described elsewhere (*23*). The wet etching technique is accurate to about ±5 μm, so the post tops are slightly irregular circles. After the etching, two inlet holes and one outlet hole were drilled into the silicon wafer using an ultrasonic drill; the spatial separation of the inlets allowed mixing to occur only within the pore network. The top of the pore network was then covered by anodically bonding a 0.7 mm thick Pyrex cover slip to the wafer (*24*). After being heated in air during anodic bonding, the silicon surfaces in the pore structure were coated with a silicon dioxide layer that is water wetting. Low dead-volume stainless steel (SS) tee fittings were fixed with epoxy to the inlet and outlet holes. SS tubing connected two syringes to two short lengths (<5 cm) of Teflon tubing, which were in turn connected to the inlet tees. Both short lengths of Teflon tubing were wrapped in anaerobic tape (Coy Laboratory Products, Inc.) to prevent O_2 from diffusing into the tubing; this maintained strictly anaerobic conditions in all degassed water purged through the inlet tubing. Teflon tubing also connected the outlet tee to a waste container. Only Teflon tubing was connected directly to inlet and outlet tees because it is flexible, and this reduced any force transferred to the tees when the micromodel was moved to and from the microscope stage.

Micromodel Experiment. The experiment had to be performed in a strictly anaerobic environment. Hence, great care was taken to make sure the system was free of oxygen initially and throughout the experiment. The micromodel, tees, and tubing were flushed with greater than 100 pore volumes of carbon dioxide to facilitate gas displacement. Next, two syringes were filled with degassed, distilled, and deionized water, and this was purged through the micromodel until no gas remained in the pore network. To degas water, it was put under a vacuum while being continually stirred for at least 24 h prior to use.

After the micromodel pore network was saturated with water, two syringes (denoted A and D) were prepared, and their solutions were purged into each of the inlets for 10 days at 8 μL/h to inoculate the micromodel. Syringe A (acceptor) contained aqueous-phase PCE at 0.2 mM; the anaerobic, chloride-free growth medium lactate at 2 mM; and the pure culture *S. multivorans*. Initially, daughter products of PCE (i.e., TCE and DCE) were also present in syringe A due to the favorable growth conditions. Syringe D (donor) contained only lactate at 2 mM. After 10 d, purging was stopped, and the syringes were replaced with two new ones. Syringe A

contained only PCE (0.2 mM) and medium; syringe D still contained lactate (2 mM). This marked the onset of stage I. From this time forward, PCE and lactate were present together only along the transverse mixing zone around the horizontal center of the micromodel pore network (stage I), and the flow rate was maintained at 8 μL/h for each syringe. This flow rate corresponds to an average linear velocity of 8.4 m/d. Velocities on this order are found in sandy aquifers.

For the next 33 d, solutions in syringes A and D or in identical replacements were continuously purged through the micromodel. In stage II of the experiment, the PCE concentration in syringe A was increased to 0.5 mM, which is slightly above observed toxicity levels of 0.3−0.4 mM for this bacteria (*25*), and maintained at this level for the next 16 d. In stage III of the experiment, the PCE concentration was doubled to 1 mM, which approaches the solubility limit of this compound. The experiment was terminated after a total of 110 d.

Effluent samples were periodically collected in $^1/_{16}$ in. diameter stainless steel tubing that was connected to the Teflon tubing attached to the outlet tee. After more than 0.5 mL of effluent accumulated in the stainless steel tubing, it was directly injected into the purge tube of a Tekmar purge-and-trap system connected to a Hewlett-Packard gas chromatograph (GC) equipped with a photoionization detector (PID) and an electrolytic conductivity detector (ELCD). Each sample was analyzed for PCE, TCE, and DCE.

To determine if biofilm growth affected flow hydrodynamics, tracer tests were performed in the micromodel just after the experiment was terminated (i.e., after 106 d) and after all biomass was removed from the pore network. Biomass was removed from the pore network by pulling concentrated sulfuric acid through the micromodel pore network and then flushing the micromodel with more than 500 pore volumes of deionized, distilled water. During a tracer test, a fluorescent dye (Alexa Fluor, Molecular Probes) dissolved in water was put in syringe A and injected into one inlet, while clean water was put in syringe D and injected into the other inlet, both at 8 μL/h. After complete tracer breakthrough, the entire micromodel was imaged using fluorescent microscopy to determine the mixing zone location.

Imaging Equipment and Image Acquisition. Micromodel images were captured with an inverted epifluroscence microscope (Epiphot 200 series, Nikon) fitted with an automated stage (Prior Scientific Instruments Inc.) and digital monochrome camera (Model Spot RT, Diagnostics Inc.). The stage and camera were connected to a personal computer and controlled by the imaging software, Metamorph (Universal Imaging Corporation). The precision of the stage in the *x*, *y*, and *z* directions is 0.1 μm.

Biofilm growth in the micromodel was imaged whenever significant changes were observed. During image acquisition, the micromodel was mounted on the motorized stage, and pictures at one vertical location were taken at 200× magnification (20× objective) using reflected light differential interference contrast (DIC) microscopy. The image resolution was 0.35 μm/pixel. At this resolution, 520 pictures were required to capture the entire 1 cm × 1 cm pore network. These were montaged into one image using the imaging software Metamorph. Images of the fluorescent tracer were taken in the same way except that fluorescence microscopy was used.

Montaged images of biomass were analyzed to determine the amount of growth over time. The negative of each image was taken. The gray scale intensity range for the biomass was determined from these images, and the pixels above and below this range were eliminated. In many images, the light reflecting off the edges of silicon posts had the same intensity range as the biomass. Pixel clusters from these regions had well-defined edges as compared to the amorphous biomass. The software was used to eliminate these regions using shape and elliptical factors for filtering. The areas with biomass growth were summed to represent the total biomass at each time step. Because total area with biological growth and not biomass was measured, only the relative or apparent increase in biomass (not the actual amount) was determined.

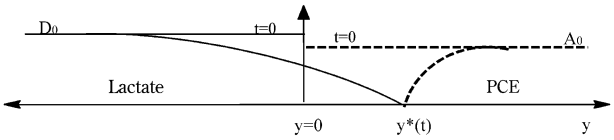

FIGURE 2. Illustration of the modeled reaction location ($y^*(t)$) between D and A. D_0 and A_0 represent the initial or influent concentrations of the donor (lactate) and the acceptor (PCE), respectively.

Model Development and Application

A new analytical solution to a simplified reactive transport model was developed to evaluate the effects of transverse hydrodynamic dispersion on the location of biomass growth. In the model, we assume that biological reaction is instantaneous when lactate and PCE mix together, that PCE and lactate mix through transverse hydrodynamic dispersion, and that biomass does not affect flow hydrodynamics. We first consider a one-dimensional transient reaction−diffusion problem in an infinite domain. A schematic is shown in Figure 2. Initially two reactants (A = acceptor = PCE; D = donor = lactate) are segregated. As the two reactants mix by diffusion, they are consumed instantaneously by the biological reaction within a very small zone located at the position denoted as $y^*(t)$. We assume that this reaction can be expressed as: $mA + nD \rightarrow$ "products", where m and n are stoichiometric coefficients. We also assume that *cis*-DCE and acetate are end products of the reaction between PCE and lactate (*20*). This yields $m = n = 1$. The moving boundary y^* separates the domain into two separate regions, each of which only contains one of the reactants.

To derive an expression for $y^*(t)$, we modify the solution of a related moving boundary problem that was presented by Feeney et al. (*26*) and Ortoleva (*27*). For each of the PCE and the lactate zones illustrated in Figure 2, we have the following governing equations:

$$\frac{\partial A}{\partial t} = E\frac{\partial^2 A}{\partial y^2} \quad D = 0 \quad y^*(t) \le y \le +\infty \tag{1}$$

$$\frac{\partial D}{\partial t} = E\frac{\partial^2 D}{\partial y^2} \quad A = 0 \quad -\infty \le y \le y^*(t) \tag{2}$$

where E is the transverse hydrodynamic dispersion coefficient. Far away from the reaction zone, we have the boundary condition

$$A(y \rightarrow +\infty, t) = A_0 \quad D(y \rightarrow -\infty, t) = D_0 \tag{3}$$

while at the reaction zone location the reactants both diminish to zero:

$$A(y^*(t), t) = D(y^*(t), t) = 0 \tag{4}$$

Within the reaction zone, the rate of reaction equals the rate at which each of the two reactants is being supplied to the zone. Thus

$$nE\frac{\partial A}{\partial y} = -\, mE\frac{\partial D}{\partial y} \tag{5}$$

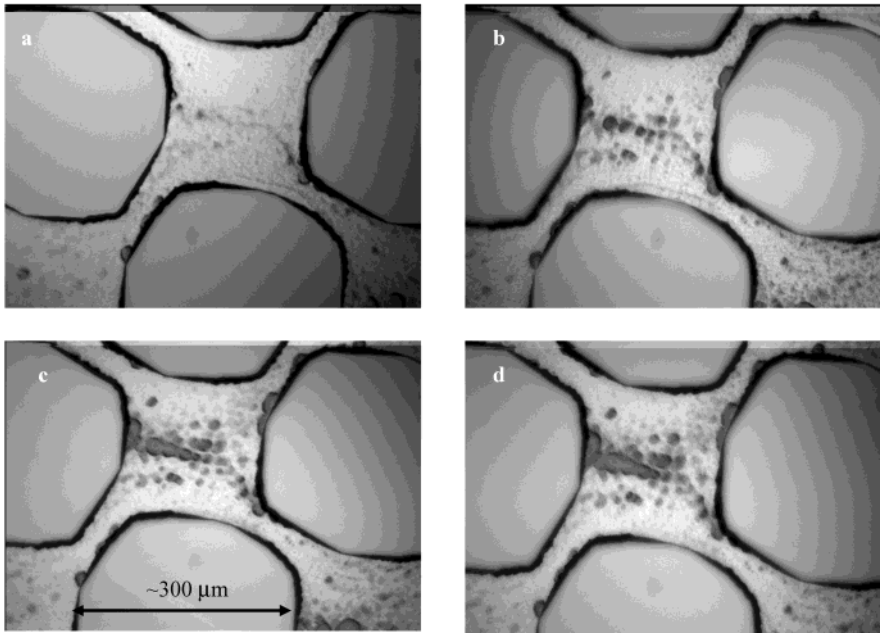

FIGURE 3. Sequential images of biomass growth from a downstream section of the pore network after (a) 25 d (stage I), (b) 32 d (stage I), (c) 39 d (stage I), and (d) 44 d (stage II). Flow is from left to right.

Feeney et al. (*26*) and Ortoleva (*27*) considered a similar problem with slightly modified boundary conditions. We followed their procedure and derived a new analytical solution for the concentration profiles in each reaction zone as well as the position of the moving boundary. Here we only give the solution for $y^*(t)$. It can be shown that

$$y^*(t) = a\sqrt{t} \tag{6}$$

where the coefficient a is given by the solution of

$$\mathrm{erf}\left(\frac{a}{2\sqrt{E}}\right) = \frac{\frac{n}{m}\frac{D_0}{A_0} - 1}{\frac{n}{m}\frac{D_0}{A_0} + 1} \tag{7}$$

It is straightforward to adapt the transient solution presented above to the steady-state reaction−diffusion problem by replacing the time variable with the hydraulic residence time. Thus, at steady state the spatial evolution of the mixing zone downstream of the inlet ($x = 0$) is given by

$$y^*(x) = a\sqrt{x/v} \tag{8}$$

where v is the pore-water velocity. Note that the derivation above assumes that both reactants have the same transverse hydrodynamic dispersion coefficient and, more importantly, that the system can be modeled at the continuum scale where the bulk pore-water velocity is one-dimensional. Transverse dispersion in two-dimensional spatially ordered porous media similar to that in our experimental micromodel has been studied theoretically by Edwards et al. (*28*) and Koch et al. (*29*). These studies show that the transverse dispersion coefficient is roughly 2−3 times the molecular diffusion coefficient for a staggered spacing of cylinders at the flow rate used in the experiment. The posts in the micromodel are not smooth cylinders, and so we may expect a slightly larger value for dispersion in our experiment. In our calculations here, we assume that $E = 2.5E_{\mathrm{mol}} = 2.5 \times 10^{-5}$ cm^2/s, where E_{mol} is the molecular diffusion coefficient. Values of E_{mol} for lacate and PCE are within a factor of 1.3 (*30*). Differences of this magnitude affect the location of the modeled reaction line by less than 10% so the average value was used.

Results and Discussion

Biomass Morphology. Images of pores with biomass growth are shown in Figures 3 and 4. Images in Figure 3 were taken near the horizontal end of the pore network (i.e., downgradient) during stages I and II, whereas those in Figure 4 were taken near the horizontal beginning of the pore network (i.e., upgradient) during stages II and III. In all cases, flow was from left to right. Biomass was observed within 1 week after stage I started. Biomass was initially present as small (i.e., much less than the pore size) amorphous clumps or aggregates in the pores (Figure 3a,b). These aggregates were oriented along the direction of flow. Over time, they grew and fused to form finger-like structures with one end attached to the silicon posts (Figure 3c,d). These fingers also fused to form thicker fingers (Figure 4a,b). In all cases, the fingers were connected to the silicon posts at the downgradient flow stagnation zones and then extended into the pore bodies. The fingers were also angled slightly toward the lactate side of the pore network (which is discussed later). In contrast to our hypothesis, significant biomass never appeared in or blocked pore throats, presumably because growth was favored in pore bodies where the shear stress was lower (relative to that in the pore throats). Also, very little biomass grew at flow stagnation zones on the upgradient side of silicon posts. A possible reason for this is that local velocities and pressures on the downgradient side of a post will tend to orient a biomass finger into the center of the pore body, where the shear is a minimum. In contrast, at the upgradient side of a post, the local velocities and pressures will act to push a biomass finger away from the pore centerline and in the direction of a pore throat, where shear forces are higher.

When conditions for growth were not favorable, such as when the PCE concentration was near saturation (i.e., 1 mM) or when only the electron donor or electron acceptor was present, the biomass fingers shrunk in size. As shown in Figure 4c,d, the first step in this process was a reduction in the density of biomass at the periphery. This was followed by sloughing off of biomass aggregates from the edges. These images were taken after the inlet PCE concentration was

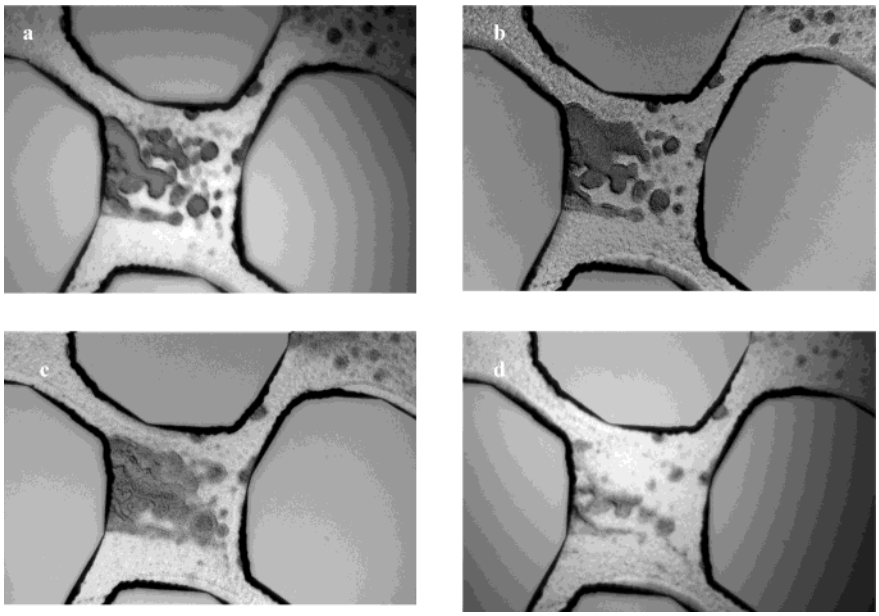

FIGURE 4. Sequential images of biomass growth from an upstream section of the pore network after (a) 44 d (stage II), (b) 51 d (stage II), (c) 63 d (stage III), and (d) 103 d (stage III). Flow is from left to right.

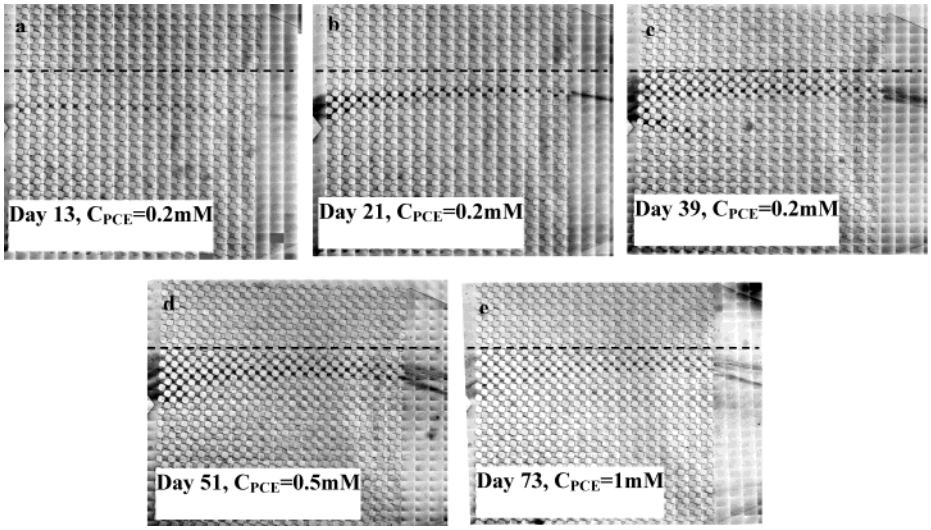

FIGURE 5. Biomass growth in the micromodel over time. The dashed line is in a fixed position and is used for reference. PCE and media were fed into the top half of the pore network, and lactate was fed into the bottom half of the pore network. Flow is from left to right.

raised to 1 mM (stage III). Also note that the biomass finger in Figure 3 is thinner than the upstream biomass finger in Figure 4. This trend could be a result of reduced nutrient availability at the downstream end of the pore matrix.

Biofilm Distribution and Growth Rates. Microbial growth in the micromodel was distributed over several pore widths transverse to the flow direction during the course of the experiment (Figure 5). The first significant growth occurred as a line, one pore body wide, that extended the length of the pore network just above the micromodel centerline (Figure 5a). Over the next few days, the line of growth migrated upward (Figure 5b) into the PCE zone, eventually extending over a width of up to five pore spaces (Figure 5c). At this time, a downward-sloped trail of biomass is evident in the outlet reservoir after the last column of pores. This biomass trail slopes downward because it goes directly to the outlet hole that is on the micromodel centerline. Also at this time, there is a small tongue of growth near the entrance of the pore network that is angled away from the rest of the biomass. This tongue appeared and disappeared over a time period of no more than 19 d (the exact time period could not be determined because of the frequency at which images were taken). While interesting, this tongue of growth did not affect the general growth pattern, and the reason for it will be addressed below.

After the PCE concentration was increased to 0.5 mM, which is slightly above the toxicity levels for the bacteria, the microbial growth responded by moving down toward the lactate side of the micromodel (Figure 5d). One possible reason for this movement is that PCE concentrations on the PCE side of the biomass may have been toxic and growth was favored on the lactate side of the micromodel. A second reason will be assessed below using the simplified model.

When the PCE concentration was increased to near-saturation values (1 mM), the biomass appears to diminish and slough-off (Figure 5e). At these high influent concentrations, it is possible that the PCE concentrations in the vicinity of the biomass increased above the toxicity levels, causing bacterial death.

Model predictions and measured biomass locations are shown in Figure 6. When PCE = 0.2 mM (i.e., $A_0 = 0.2$ mM), the model predicts that the optimal reaction line will start

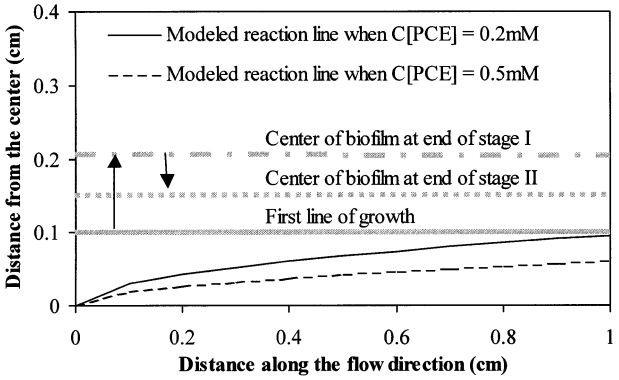

FIGURE 6. Observed biomass growth locations and the predicted reaction locations based on model equation (*8*).

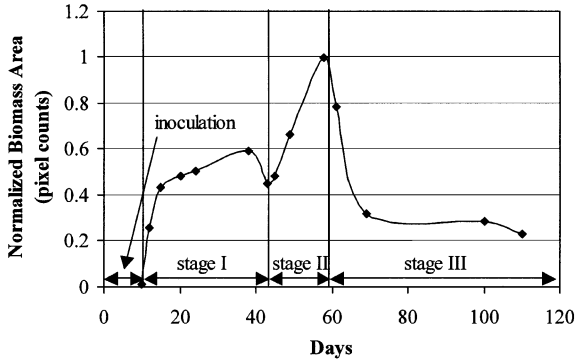

FIGURE 7. Biomass growth observed in the micromodel based on the number of pixels containing biomass.

at the micromodel centerline in the first column of pores and asymptotically move upward to a distance ~0.1 cm from the centerline in the last column of pores. The initial biomass in the pore network has less curvature than the model predicts; it extends across the length of the pore network approximately 0.1 cm above the micromodel centerline.

There are at least two factors that likely contribute to the discrepancy between initial biomass growth and the predicted reaction line. First, with the model we assume uniform flow in a fluid continuum, whereas the pore network in the micromodel imposes a nonuniform and tortuous flow geometry. Second, in the mathematical model, the reaction-zone location is controlled by dispersive mixing of the two reactants. However, biomass may grow toward the more limiting reactant and thereby affect the location of the reaction zone. Despite these significant differences, the modeled reaction line and measured biomass location are both above the horizontal center of the micromodel pore structure and they intersect. This suggests that, at early time, transverse hydrodynamic dispersion largely controls PCE and lactate mixing and the location of microbial growth.

In contrast to the modeled reaction line, the biomass growth continued to move upward over time. After 40 d, the biomass growth reached a distance ~0.21 cm above the centerline. The migration of biomass upward during the experiments indicates that PCE was the limiting nutrient during this process. We postulate that PCE was limited because it diffused more slowly through the biofilm than lactate because of retardation. This can be expected since PCE, but not lactate, will absorb to extracellular polymers and the membrane fraction of microbial cells that are composed of lipids. This is contrary to our hypothesis that only transverse hydrodynamic dispersion will control the mixing zone location between PCE and lactate and, therefore, the location of biomass growth.

After stage I, the PCE concentration was increased to 0.5 mM. Under this new condition the biomass growth shifted downward by approximately 0.05 cm, indicating that PCE was less limiting. The modeled reaction line also shifted down, but the amount of the shift was slightly less than 0.04 cm. This indicates that when the inlet concentration of PCE was increased to 0.5 mM, transverse hydrodynamic dispersion of PCE into the reaction zone increased and shifted the zone of biomass growth to the lactate side of the micromodel. It is important to note that at this time the absolute locations for the modeled reaction line and the biomass growth did not coincide. This occurred because the line of biomass growth had previously grown above the modeled reaction line when PCE = 0.2 mM. Thus, flow and transport of PCE and lactate were affected by previous growth.

The transverse hydrodynamic dispersion coefficient was used to calculate the distance (y_d) over which transverse dispersion occurs using an analytical solution (*31*) for diffusion [$C/C_0 = 1/2$ erfc ($y_d/(2\sqrt{Ex/v})$)] and assuming this distance is between $C/C_0 = 0.1$ and 0.9. The distance over which transverse dispersion occurs scales with x; y_d increases from 0.13 to 0.18 cm (i.e., ~3−4 pore widths) as x increases from 0.5 to 1 cm. The transverse width of the biofilm is initially smaller than 2 pore widths but exceeds this at a later time. This indicates that the reaction rate is fast relative to the rate of transverse dispersion, at least at early time. At later time, when biomass occupies up to five pore bodies across, it is not clear if the reaction rate slowed, if the presence of biomass caused the rate of transverse mixing to increase, or if residual material from the biomass makes it appear that the reaction zone is wider than the transverse dispersion distance.

On the basis of the number of pixels containing biological growth, the amount of biomass was quantified over time, and the results are shown in Figure 7. During stage I, biomass increased linearly, leveled off, and then dropped slightly toward the end. Similarly, Peyton and Characklis (*32*) observed that biofilms reached a steady-state condition in which new growth was equivalent to biomass sloughing. During stage II, biomass again increased linearly. During stage III, biomass dropped sharply until a relatively constant level was reached. This pattern of increase in biomass contrasts the exponential growth observed in batch cultures and is likely a direct result of the nutrient mass transfer limitations and sloughing that occur in the micromodel.

Initial doubling times of the biomass were calculated for the linear growth regions by determining the amount of time required for the initial biomass concentration to double one time. During stage I, this initial doubling time was ~4.5 h. Although not comparable over a long period of time, this initial rate is similar to the doubling time of 2.5 h measured by Sholz-Muramatsu et al. (*25*) in exponentially growing batch cultures of the same microorganism. At the beginning of stage II, the time for the biomass to double increased to ~108 h. Possible reasons for this increase are that there is more detachment of new biomass at greater biomass concentrations and that some existing biomass was no longer active because it was limited in either PCE or lactate.

On the basis of the observed growth rates, we hypothesize that for any initial condition an equilibrium point exists where no further growth will be observed. This was actually apparent when growth plateaued in stage I. This was the point where the rate of growth was equal to the rate of loss; therefore, no net gain in biomass mass was observed. This result has implications for bioremediation because apparent microbial growth rates will likely slow when thick regions of biomass develop.

The final drop in biomass during stage III indicates that PCE concentrations near the solubility limit were toxic to

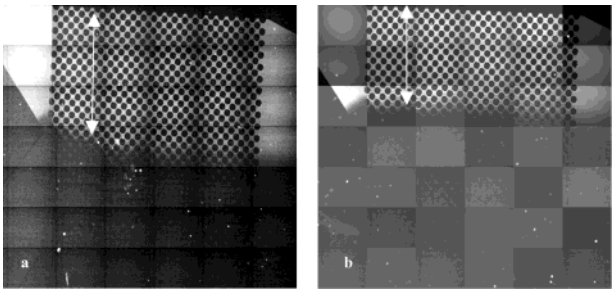

FIGURE 8. Mixing zone location in the (a) absence and (b) presence of microbial growth determined from a fluorescent tracer experiment.

the bacteria. The leveling off of biomass observed at the end of this stage indicates that extracellular polymers and other remnants of previous growth remained in the pore network after the bacteria appeared to die off.

Mixing Zone Location. A fluorescent tracer experiment was performed to determine if the biomass growth affected the mixing location between PCE and lactate (Figure 8). In the absence of biomass (Figure 8a), the region that shows fluorescence starts at the centerline of the micromodel near the inlet and then moves downward toward the outlet. Transverse dispersion causes the region of fluorescence to grow, and the results indicate that the mixing zone is approximately along the centerline of the micromodel. In the presence of biological growth (Figure 8b), the region that shows fluorescence is confined to the area above where the most dense biomass growth occurred. It is important to note that this image was taken at the end of stage III, when the observed biomass was much less than during stage II (Figure 7). In agreement with our hypothesis, this indicates that biomass material was dense enough to cause a significant reduction in permeability and transverse dispersion. The reduction in permeability was verified by observations of colloidal precipitates in the trace salts/metals media being diverted by and moving around the biomass during the experiment. These results suggest that the presence of biomass in the micromodel experiments significantly changed the mixing location between PCE and lactate. As a result, PCE was primarily confined to the area above the biomass and lactate primarily occupied the area below the biomass. Because the flow rate of PCE and lactate were the same and because PCE flow was confined to a smaller cross-sectional area than lactate flow, the pressure on the PCE side of the pore network was higher. This pressure difference likely caused the fingers of growth in individual pores to angle slightly down toward the lactate side of the micromodel (Figures 3 and 4). This pressure difference also likely caused PCE to temporarily break through the main line of biomass and create a temporary tongue of growth as described with Figure 5. These results indicate that, during bioremediation, biomass growth can change the extent and location of the reaction zone along plume margins.

Biomass Activity. Effluent samples were analyzed to determine biomass activity. In the absence of biomass in the micromodel, effluent PCE concentrations were as small as 10% of influent PCE concentrations. This indicated significant solvent losses occurred during sampling. The total flow rate through the micromodel was 16 μL/h. Collected effluent samples were greater than 500 μL. Each sample took greater than 30 h to collect. We believe that solvent losses occurred because long sampling times allowed solvents to evaporate from the end of the stainless steel sample tube and to diffuse through the Teflon tubing that connected the micromodel effluent tee to the stainless steel sample tubing. Regardless of these losses, solvent concentrations were still well above detection limits, and overall activity was assessed.

During both stage I and stage II of the experiment, greater than 96% of the solvent mass in the effluent was DCE. This indicates that during this time bacteria in the micromodel and effluent tubing were actively degrading PCE to DCE. Imaging results (Figure 5) and the growth curve (Figure 7) indicate that biomass in the pore network responded to changing PCE concentrations. This and the measured DCE concentrations support the conclusion that biomass in the micromodel pore network actively respired PCE to DCE. During stage III, greater than 87% of the solvent mass in the effluent was PCE, with the remainder being DCE. Whether the DCE was due to continued activity or slow desorption from inactive biomass was not clear. Regardless, these results indicate that bacteria died off during this period and that very little or no further activity occurred. This has implications in the field if flow fields change and previously established microorganisms are subject to near saturated concentrations of PCE.

In summary, there are three main results from this work. First, the anaerobic bacterium *S. multivorans* grew as fingers connected to silicon posts at downgradient flow stagnation zones and then extended into adjacent pore bodies. Biomass did not grow in pore throats or in stagnation zones at the upgradient side of silicon posts as expected, possibly because shear stress was unfavorable. Second, transverse hydrodynamic dispersion affects and can control nutrient mixing along plume margins, especially at early time when biomass is low. However, when significant biomass develops, preferential retardation of one chemical over another may occur. Third and last, biomass along a transverse mixing zone clearly affects permeability and the location of the mixing zone. Further research is needed to determine how the growth of *S. multivorans* responds to other system parameters such as electron donor type and starvation, how biomass morphology affects dechlorination rates, and if the results observed here are general to other bacterium and to mixed cultures.

Acknowledgments

This work was primarily supported by the National Science Foundation Biogeochemistry Program under Grant CTS-9905730. Support for the purchase of the microscope imaging system was provided by the University of Illinois Research Board. The authors thank Cheema Chomsurin for help with micromodel fabrication and digital image analysis, Mary Jo Kirisits for reviewing an earlier version of this manuscript, and three anonymous reviewers for helpful comments.

Literature Cited

(1) Semprini, L.; Hopkins, G. D.; Roberts, P. V.; McCarty, P. L. *J. Hazard. Mater.* **1992**, *32*, 145−162.
(2) Kao, C. M.; Lei, S. E. *Water Res.* **2000**, *34* (3), 835−845.
(3) Vera, S. M.; Werth, C. J.; Sanford, R. A. *Biorem. J.* **2001**, *5* (3), 169−181.
(4) Koenigsberg, S. S.; Sandefur, C. A. *Rem. J.* **1999**, *10* (1), 31−53.
(5) Cirpka, O. A.; Frind, E. O.; Helmig, R. *J. Contam. Hydrol.* **1999**, *40*, 159−182.
(6) Thornton, S. F.; Lerner, D. N.; Banwart, S. A. *J. Contam. Hydrol.* **2001**, *53*, 199−232.
(7) Grane, F. E.; Gardner, G. H. F. *J. Chem. Eng. Data* **1961**, *6* (2), 283−287.
(8) Klenk, I. D.; Grathwohl, P. *J. Contam. Hydrol.* **2002**, *58*, 111−128.
(9) Oya, S.; Valocchi, A. J. *Water Resour. Res.* **1998**, *34* (12), 3323−3334.
(10) Raje, D.; Kapoor, V. *Environ. Sci. Technol.* **2000**, *34*, 1234−1239.
(11) Thullner, M.; Mauclaire, L.; Schroth, M. H.; Kinzelbach, W.; Zeyer, J. *J. Contam. Hydrol.* **2002**, *58*, 169−189.
(12) Baveye, P.; Vandevivere, P.; Hoyle, B. L.; DeLeo, P. C.; de Lozada, D. S. *Crit. Rev. Environ. Sci. Technol.* **1994**, *28* (2), 123−191.
(13) Cunningham, A. B.; Characklis, W. G.; Abedeen, F.; Crawford, D. *Environ. Sci. Technol.* **1991**, *25* (7), 1305−1311.
(14) Rittmann, B. E. *Water Resour. Res.* **1993**, *29* (7), 2195−2202.
(15) Kim, D.-S.; Fogler, H. S. *Biotechnol. Bioeng.* **2000**, *69* (1), 47−56.

(16) Paulsen, J. E.; Oppen, E.; Bakke, R. *Water Sci. Technol.* **1997**, *36* (1), 1−9.
(17) Dupin, H. J.; McCarty, P. L. *Environ. Sci. Technol.* **2000**, *34* (8), 1513−1520.
(18) Dupin, H. J.; Kitanidis, P. K.; McCarty, P. L. *Water Resour. Res.* **2001**, *37* (12), 2981−2994.
(19) Vayenas, D. V.; Michalopoulou, E.; Constantinides, G. N.; Pavlou, S.; Payatakes, A. C. *Adv. Water Resour.* **2002**, *25*, 203−219.
(20) Neumann, A.; Scholz-Muramatsu, H.; Diekert, G. *Arch. Microbiol.* **1994**, *162* (4), 295−301.
(21) Sanford, R. A.; Cole, J. R.; Tiedje, J. M. *Appl. Environ. Microbiol.* **2002**, *68*, 893−900.
(22) Wan, J.; Wilson, J. L. *Water Resour. Res.* **1994**, *30* (1), 11−23.
(23) Madou, M. J. *Fundamental of Microfabrication*; CRC Press: Boca Raton, FL, 1997.
(24) Albaugh, K. B.; Rasmussen, D. H. *J. Am. Ceram. Soc.* **1992**, *75* (10), 2644−2648.
(25) Scholz-Muramatsu, H.; Neumann, A.; Messmer, M.; Moore, E.; Diekert, G. *Arch. Microbiol.* **1995**, *163* (1), 48−56.
(26) Feeney, R.; Schmidt, S. L.; Strickholm, P.; Chadam, J.; Ortoleva, P. *J. Chem. Phys.* **1983**, *78* (3), 1293−1311.
(27) Ortoleva, P. *Geochemical Self-Organization*; Oxford University Press: Oxford, 1994.
(28) Edwards, D. A.; Shapiro, M.; Brenner, H.; Shapira, M. *Trans. Porous Media* **1991**, *6*, 337−358.
(29) Koch, D. L.; Cox, R.; Brenner, H.; Brady, J. F. *J. Fluid Mech.* **1989**, *200*, 173−188.
(30) Wilke, C. R.; Chang, P. *AIChE J.* **1955**, *1* (2), 264−270.
(31) Crank, J. J. *The Mathematics of Diffusion*, 2nd ed.; Oxford University Press: Oxford, 1975.
(32) Peyton, B. M.; Characklis, W. G. *Water Sci. Technol.* **1992**, *26* (9−11), 1995−1998.

Received for review March 25, 2003. Revised manuscript received September 21, 2003. Accepted September 22, 2003.

ES034271W